Macromolecules

Article

pubs.acs.org/Macromolecules

Discovery of β-Form Crystal Structure in Electrospun Poly[(*R*)-3-hydroxybutyrate-*co*-(*R*)-3-hydroxyhexanoate] (PHBHx) Nanofibers: From Fiber Mats to Single Fibers

Liang Gong,[†] D. Bruce Chase,[†] Isao Noda,[†,‡] Jinglin Liu,[†] David C. Martin,[†] Chaoying Ni,[†] and John F. Rabolt*[,†]

[†]Department of Materials Science and Engineering, University of Delaware, Newark, Delaware 19716, United States

[‡]MHG, Inc., Bainbridge, Georgia 39817, United States

ABSTRACT: For the first time the strain-induced metastable β-form crystal structure, with the extended chains adopting a planar zigzag conformation, was discovered in the macroscopically aligned electrospun nanofibers of poly[(*R*)-3-hydroxybutyrate-*co*-(*R*)-3-hydroxyhexanoate] (PHBHx) collected across the air gap on aluminum foil and on the tapered edge of a high-speed rotary disk. The presence of the β-form crystal structure in the fiber mats was confirmed by wide-angle X-ray diffraction (WAXD) and Fourier transform infrared spectroscopy (FTIR). In addition, selected area electron diffraction (SAED) and AFM-IR were utilized to investigate the morphological and structural details of individual electrospun nanofibers. The SAED results confirmed a significant influence of the collection method on the crystal structure as well as the orientation level of the molecular chains in the crystals. The AFM-IR spectra of the single nanofibers matched well with the traditional FTIR spectra, but the finer features in the AFM-IR spectra were more distinct and better resolved. Based on the experimental results, new mechanisms for the generation of the β-form crystalline structure in electrospun PHBHx nanofibers are proposed.

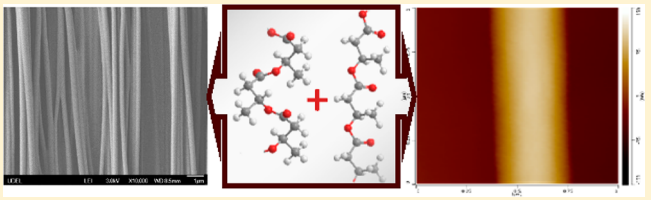

INTRODUCTION

Polyhydroxyalkanoates (PHAs) are a class of biodegradable and biocompatible aliphatic polyesters synthesized by a variety of bacteria as intracellular carbon and energy storage materials. They have attracted scientific attention for their promising environmental, electrical, pharmaceutical, and biomedical applications.[1] Among PHAs, poly(3-hydroxybutyrate) (PHB) homopolymer is the most common type and has been extensively studied over the past 30 years. However, due to the near perfect stereoregularity, bacterially produced PHB has very high crystallinity (>60%) and a melt temperature range (ca. 180 °C) near its thermal decomposition temperature.[2] The constraint of the difficult-to-process thermal properties and rigid and brittle nature of the material are major obstacles to most standard applications. Copolymerization with other small monomer units, such as 3-hydroxyvalerate (3HV), was attempted with relatively little success in improving the properties. This surprising result arises from the fact that 3HB and 3HV units are isodimorphous, with 3HV units being incorporated into the PHB crystalline lattice.[3] Recently, in order to substantially enhance the properties of PHB, a small amount of hydroxyalkanoic acid monomers with longer side chains, such as 3-hydroxyhexanoate (3HHx), was copolymerized with 3HB units to avoid the isodimorphism and reduce the rigidity and brittleness of the resultant copolymer. These medium chain length (mcl) branches act as molecular defects, disrupting the excessive regularity of the polymer chain and consequently lowering the crystallinity and melting point (T_m).[4] The resultant random copolymer, poly[(*R*)-3-hydroxybutyrate-*co*-(*R*)-3-hydroxyhexanoate] (PHBHx), becomes soft and flexible as the 3HHx content increases and results in properties similar to linear low-density polyethylene (LLDPE).[4] Many properties of PHBHx, including chemical, thermal, and mechanical properties, can be adjusted by changing the comonomer content.

It has been established that PHB and poly[(*R*)-3-hydroxybutyrate-*co*-(*R*)-3-hydroxyvalerate] (PHBV, a PHB-based random copolymer) can exhibit two different crystalline polymorphs, the α-form and β-form, depending on processing conditions. The α-form is the most common crystal structure of the PHB or PHBV polymers obtained from typical crystallization processes, such as melt or solution crystallization. In this crystal polymorph, the molecular chains adopt a left-handed 2_1 helical conformation. The unit cell is orthorhombic with a space group of $P2_12_12_1$-D_2[4] and lattice parameters of a = 0.576 nm, b = 1.320 nm, and c (fiber period) = 0.596 nm.[5] The other crystal polymorph, the β-form crystal, is recognized as a strain-induced paracrystalline structure with highly extended chains.[6] In the β-form, the chains adopt a twisted planar zigzag conformation, which is a nearly fully extended chain conformation. The unit cell is also orthorhombic with lattice parameters of a = 0.528 nm, b = 0.920 nm, and c (fiber period)

Received: March 26, 2015
Revised: July 30, 2015

DOI: 10.1021/acs.macromol.5b00638
Macromolecules XXXX, XXX, XXX−XXX

= 0.470 nm.[7] This metastable crystal structure, which can be annealed back to the α-form at 130 °C,[8] was first observed in hot-drawn PHB thin films[5] and later was found in cold-drawn PHBV thin films.[9] In particular, this β-form was found in a cold-drawn amorphous film,[9] indicating that the generation of the β-form does not require prior alignment of the α-form crystals. Over the following 10 years, the metastable β-form has been successfully generated in thin films[8,10−12] or melt-spun fibers[13−20] of PHB and PHBV under different postprocessing conditions, where the films or fibers were highly stretched, although the draw ratios may vary. It is reported that the β-form remained relatively unchanged for months at room temperature,[10,15] suggesting that this crystal structure does not undergo secondary crystallization.

The β-structure has long been accepted to originate from the orientation of the free chains in the amorphous phase between the α-form lamellar crystals.[12,15,16,21] When experiencing high stretching forces, the tie molecules between the lamellar crystals will be strongly extended and orient along the stretching direction. As long as the free chains adopt a planar zigzag conformation, they would pack and form the β-structure. The generation of the β-form crystal structure has a large effect on various properties of the material, including the mechanical properties,[10,11,13−15,17] biodegradability,[16,22] and piezoelectric response.[23] It would be interesting to explore the possibility of generating this strain-induced metastable structure also in PHBHx in order to further broaden the range of applications.

Electrospinning is an effective and versatile technique, utilizing electrostatic forces to draw the solutions or melts of many different macromolecular systems to produce nanofibers (10 nm to 5 μm). Such fibers find applications in areas including composites, tissue engineering, energy storage and conversion, sensors, and filtration systems.[24−29] Efforts have been made to elucidate the strong electrically driven stretching forces during the electrospinning process. The total draw ratio is estimated to be as high as 25 000.[30] In addition, one can introduce additional stretching forces on the fibers during fiber deposition by using modified collectors, such as rotating collectors (rotary drum, rotary disk, etc.)[31−37] and gapped collectors (two charged metallic rods or plates separated by an insulated gap),[38−42] eventually obtaining macroscopically aligned fibers along the roll-up direction or across the gap. These strong stretching forces, together with extremely rapid solvent evaporation, have been observed to induce formation of metastable phases or crystalline polymorphs.[32,33,43] Therefore, electrospinning would be an interesting choice of processing technique that might induce the metastable β-structure in PHA nanofibers. In fact, the β-structure was found in PHB nanofibers electrospun from dilute polymer solutions via conventional electrospinning techniques.[22] Later, this metastable crystal structure was observed in the electrospun PHBV fibers collected on a rotary drum.[31] However, the existence of the β-form in electrospun PHBHx has not yet been reported. Actually, there has been no report, until now, of the introduction of the β-polymorph in any form of PHBHx.

In this study using two modified collectors, i.e., an aluminum foil with a rectangular air gap and a rotary disk with a tapered edge, we have succeeded in obtaining the β crystalline polymorph in macroscopically aligned electrospun PHBHx nanofibers. For fiber mats, the fiber morphology, crystal structure, and chain conformation were characterized by scanning electron microscopy (SEM), wide-angle X-ray diffraction (WAXD), and transmission Fourier transform infrared spectroscopy (FTIR). In addition, with the aid of selected area electron diffraction (SAED) and AFM-IR, we were able to investigate the structure and orientation within PHBHx nanofibers at the single fiber scale.

EXPERIMENTAL SECTION

Materials. Poly(3-hydroxybutyrate-*co*-3-hydroxyhexanoate) (PHBHx) with 3.9 mol % Hx content (M_w = 843 000 g/mol, PDI = 2.2) was supplied by the Procter & Gamble Company. The polymer was purified by dissolving in chloroform followed by filtration and subsequent precipitation in hexane. The solvent, 1,1,1,3,3,3-hexafluoro-2-propanol (HFIP), was purchased from Sigma-Aldrich and used as received.

Electrospinning. A 1 wt % electrospinning solution was prepared by dissolving the purified PHBHx into HFIP and stirring at 60 °C overnight to ensure complete dissolution. As part of our experimental protocol for electrospinning nanofibers, the polymer solution was loaded into a 3 mL BD plastic syringe with a 21 gauge stainless steel needle, which was connected to the positive terminal of a high-voltage supply held at 10 kV. Two different negatively charged collectors, a parallel-electrode collector and a rotary disk collector, were used to collect electrospun nanofibers with desired morphologies. For the parallel-electrode collector, a rectangular slot was cut in a piece of aluminum foil, leaving the slot as a 35 mm × 10 mm air gap. For the rotary disk collector, the disk was designed to have a tapered edge with half angle of 30° in order to create a converging electric field. The angular velocity of the rotary disk was set to 3500 rpm, corresponding to a linear velocity of 1117 m/min at the edge of the disk. The applied voltage between the needle and the collectors was 25 kV. The working distance and solution supply rate were 25 cm and 0.5 mL/h, respectively. All the electrospun mats were dried in vacuum for 24 h to remove any residual solvent prior to further investigation.

Characterization. *Fiber Mats.* The morphology of the electrospun PHBHx nanofibers was observed using a field-emission scanning electron microscope (SEM, JEOL JSM 7400F) at an accelerating voltage of 3.0 kV. Fiber diameters were measured using ImageJ software. Wide-angle X-ray diffraction (WAXD) measurements were carried out under ambient conditions using a Rigaku Ultima (IV) instrument operating at 44 kV and 40 mA with Cu Kα (λ = 1.5418 Å) as the X-ray source. Scans were performed in a 2θ range of 10°−40° at a speed of 1°/min and a sample step of 0.1°. The Fourier transform infrared (FTIR) spectra were collected using a Thermo Nicolet NEXUS 670 at room temperature in transmission mode. For each sample, 128 scans were signal-averaged at 4 cm^{-1} spectral resolution.

Single Fibers. Selected area electron diffraction (SAED) patterns and bright-field images were recorded by a transmission electron microscope (TEM, Tecnai G^2 12) with a low-dose CCD camera at an accelerating voltage of 120 kV. The nanofibers were deposited on 300 mesh copper grids coated with lacey carbon film to reduce specimen damage. When performing the SAED experiment, the diffraction patterns were obtained at a fixed camera length of 2.1 m, and the TEM images were taken at a constant magnification of 97 000. A thin layer of gold polycrystals was sputtered on each of the copper grid before the deposition of the fibers, which was used to calibrate the camera constant and correct any system distortion.

The high-resolution AFM images and IR spectra of single electrospun fibers were acquired with a NanoIR2 AFM-IR (Anasys Instruments). In order to maintain a good contact between the sample and substrate, PHBHx nanofibers were electrospun directly on silicon wafer substrates that are transparent in the mid-IR region from 900 to 3600 cm^{-1}. The NanoIR spectra were collected with a spectral resolution of 2 cm^{-1}, coaveraging 256 cantilever ringdowns for each data point.

RESULTS AND DISCUSSION

Studies on Fiber Mats. In recent years, many studies have illustrated the huge impact of the collectors on fiber morphologies, macroscopic alignment, and molecular orienta-

DOI: 10.1021/acs.macromol.5b00638
Macromolecules XXXX, XXX, XXX−XXX

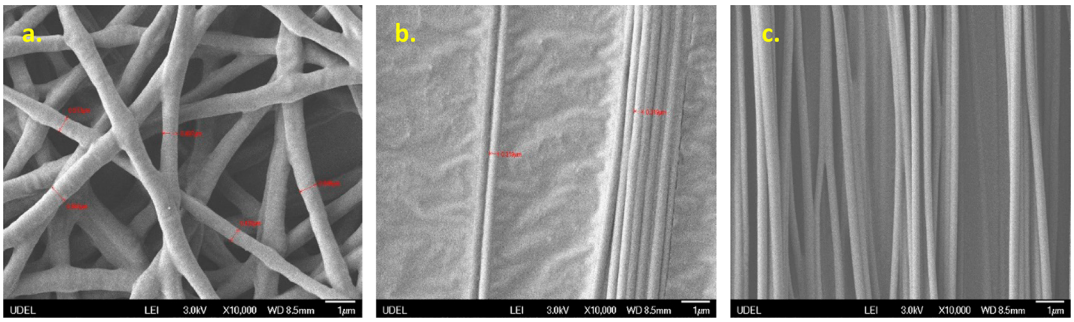

Figure 1. SEM images of electrospun PHBHx fibers collected (a) on the aluminum foil off the air gap, (b) across the air gap, and (c) on the rotary disk.

tion.[31−33,35,40] The morphologies of electrospun PHBHx nanofibers collected using different collectors, while keeping the other electrospinning parameters the same, were examined with SEM, and the images are shown in Figure 1. The SEM images clearly show how the collectors affect the fiber morphology. Because of the bending instability in the whipping region, the fibers collected on the aluminum foil off the gap are randomized (Al foil random fibers, Figure 1a), while the fibers collected across the air gap (air gap aligned fibers, Figure 1b) and on the tapered edge of the rotary disk (rotary disk aligned fibers, Figure 1c) are well-aligned. Furthermore, the average diameter of the aligned fibers (270 ± 20 nm) was much smaller than that of the Al foil random fibers (500 ± 30 nm), indicating additional stretching and drawing during formation. It has long been accepted that under rotating collection the electrospun fibers were further stretched and aligned toward the rollup direction. However, in the case of the air gap aligned fibers, the stretching is caused by the electrostatic attractive forces between the positive residual charges on the fibers and the negative charges accumulated on the gap edge. These attractive forces, in concert with the repulsive forces between the residual charges on the undischarged fibers in the air gap, result in macroscopic alignment of the fibers.[44]

In this study, the molecular orientation in the fiber mats was characterized by polarized Fourier transform infrared spectroscopy (p-FTIR). P-FTIR has been widely used to study the molecular orientation and conformational changes of polymer chains during electrospinning.[31,40] For FTIR spectra with the incident infrared beam polarized in certain directions, a high absorbance intensity will be measured if the change in dipole moment of the vibration has a component along the electric vector of the incident beam. Figure 2 shows the parallel and perpendicular p-FTIR spectra of the Al foil random fibers (Figure 2a), air gap aligned fibers (Figure 2b), and rotary disk aligned fibers (Figure 2c). As shown in the figure, the p-FTIR spectra for the aligned fibers in two mutually perpendicular directions exhibited a clear difference in absorbance intensity, which indicated the presence of molecular orientation of the PHBHx polymeric chains. In order to quantify this microscopic orientation, the normalized dichroic difference (NDD) of some characteristic peaks was calculated using the equation (assuming uniaxial symmetry)

$$\mathrm{NDD} = \frac{A_{\parallel} - A_{\perp}}{A_{\parallel} + 2A_{\perp}}$$

where $A_{\parallel}$ is the parallel-polarized infrared absorbance intensity and $A\perp$ is the perpendicular-polarized infrared absorbance intensity relative to the macroscopic fiber axis. As seen from this equation, the NDD ranged from −1/2 to 1 with NDD = 0 when the sample is isotropic. As listed in Table 1, the NDD for the carbonyl stretch was calculated as 0.001, −0.134, and −0.100 for the Al foil random fibers, air gap aligned fibers, and rotary disk aligned fibers, respectively. NDD < 0 indicates that the absorbance intensity of C═O is lower when the electric vector of the incident infrared beam is parallel to the fiber axis compared to that when the vector is perpendicular to the fiber axis ($A_{\parallel} < A\perp$). This result suggested that the carbonyl bond exhibited a perpendicular orientation to the fiber axis, and polymer chains were oriented along the fiber axis because the carbonyl bond is approximately perpendicular to the molecular backbone as anticipated by its chemical structure. As the NDD of carbonyl bond approaches −1/2, the chains are more oriented along the fiber axis. On the other hand, NDD > 0 for the C−O−C bond along the molecular backbone suggests that the C−O−C bonds were oriented approximately parallel to the fiber axis. As the NDD of C−O−C bond approaches unity (1.0), the chains are more oriented along the fiber axis. From Table 1 we see that the air gap aligned fibers had the lowest NDD (highest absolute value) for C═O stretching and the highest NDD for C−O−C stretching, which suggests that the air gap aligned fibers had the highest level of chain orientation along the fiber axis. Particularly, it is noted that the NDDs of the three bands were always around 0 for the Al foil random fibers. This result is due to the lack of macroscopic alignment of the fibers. Under these conditions, nothing can be said about the degree of chain alignment within the individual fibers.

The crystal morphology of electrospun PHBHx nanofibers was examined by WAXD and FTIR. Figure 3 shows the WAXD profiles of the Al foil random fibers, air gap aligned fibers, and rotary disk aligned fibers. In all profiles, diffraction peaks assigned to the α-form with a 2_1 helical conformation were observed.[22,45,46] Furthermore, in the WAXD profiles of the air gap aligned fibers and rotary disk aligned fibers, a diffraction peak assigned to the β-form with a planar zigzag chain conformation was observed at 2θ = 19.6°.[9,13,16,22] As is apparent, the rotary disk aligned fibers had significantly more β-form than the air gap aligned fibers. For display purposes, the intensity of $\alpha(020)$ at 2θ = 13.7° in all the profiles was normalized to unity. Considering that no β-form was found in the Al foil random fibers, this extended chain conformation must be induced by the two modified collection methods where macroscopically aligned fibers were obtained since the different collection strategies (on an air gap vs on a rotary disk rotating at 3500 rpm) involve substantially different stretching forces on the fiber and a corresponding increase in the amount of β-form produced in the latter.

DOI: 10.1021/acs.macromol.5b00638
Macromolecules XXXX, XXX, XXX−XXX

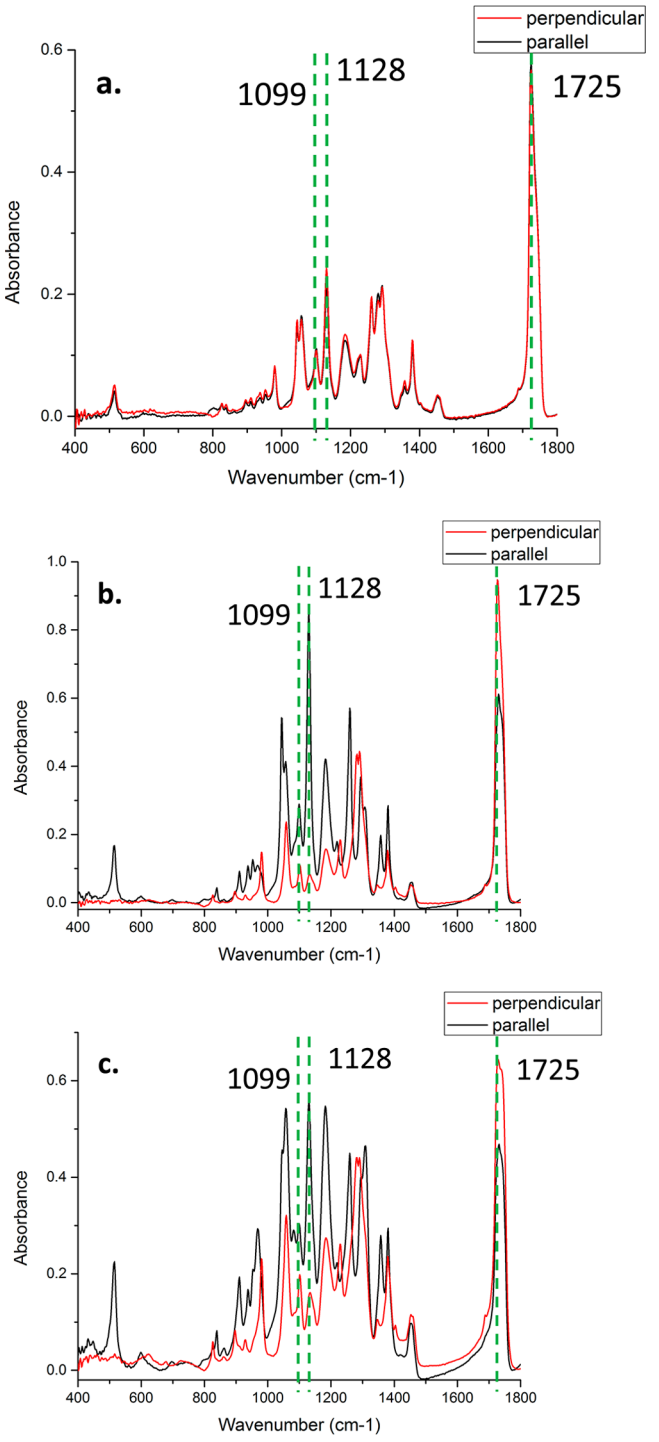

Figure 2. Polarized FTIR spectra of the Al foil random fibers (a), air gap aligned fibers (b), and rotary disk aligned fibers (c). The incident IR beam is polarized in two mutually perpendicular directions which are perpendicular (red) and parallel (black) to the aligned fiber axis.

Table 1. Normalized Dichroic Difference (NDD) of Different Vibrational Bands

vibration band (cm^{-1})	normalized dichroic difference		
	Al foil	air gap	rotary disk
1725 (C═O stretching)	0.006	−0.134	−0.100
1128 (symmetric C−O−C stretching)	−0.009	0.758	0.453
1099 (asymmetric C−O−C stretching)	0.009	0.348	0.151

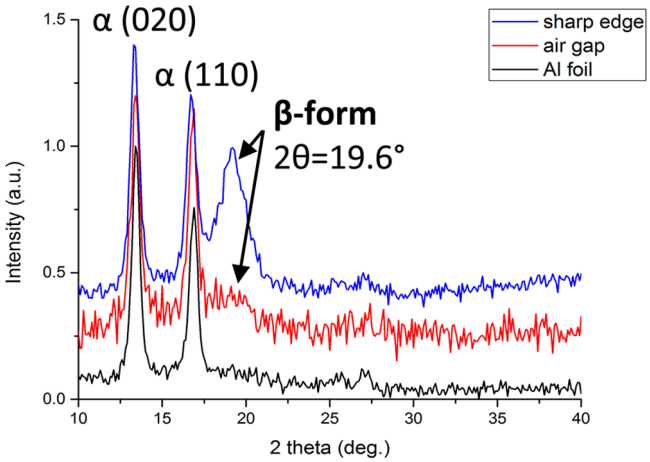

Figure 3. WAXD profiles of electrospun PHBHx fibers obtained using different collectors.

The introduction of the planar zigzag chain conformation in the fibers collected across a gap or on a rotating disk was further confirmed by transmission FT-IR spectra (Figure 4). The C═O stretching in PHAs is strongly correlated with the polymer backbone conformation.[31] As seen in Figure 4a, the C═O stretching band of the off-gap random fibers can be

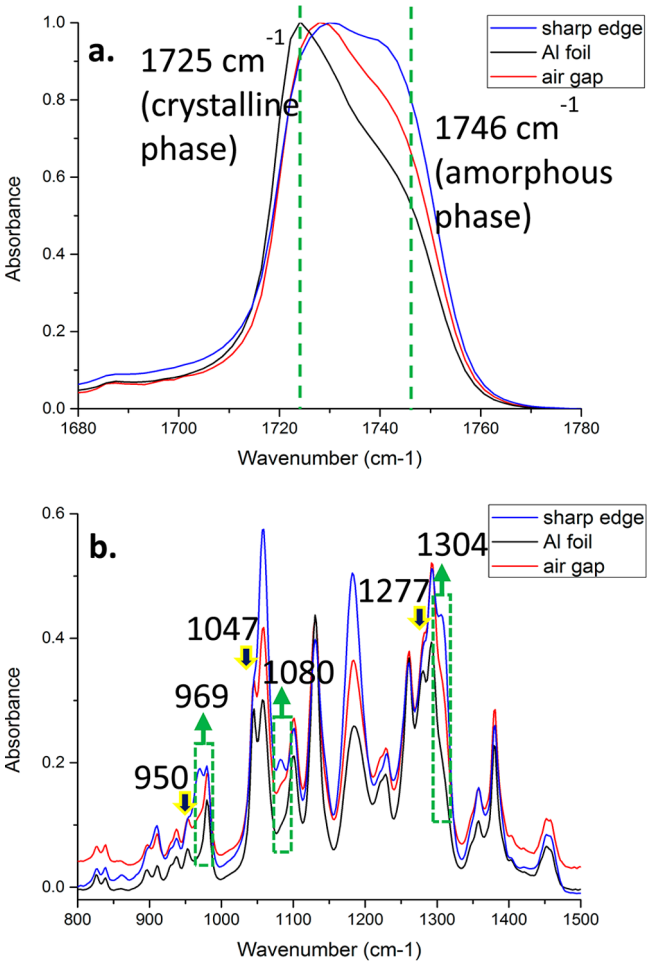

Figure 4. FT-IR spectra of off-gap random fibers, in-gap aligned fibers, and rotary disk aligned fibers in (a) C═O stretching region and (b) C−O−C stretching region.

DOI: 10.1021/acs.macromol.5b00638
Macromolecules XXXX, XXX, XXX−XXX

resolved into an intense peak at 1725 cm^{-1} corresponding to the crystalline phase and a weak shoulder at 1746 cm^{-1} corresponding to the amorphous phase. As the amount of the β-form increased, going from random fibers to aligned fibers (normalized WAXD result), the peak at 1725 cm^{-1} became broader and shifted to higher frequency, while the shoulder at 1746 cm^{-1} showed an increase in its relative intensity and shifted to lower frequency. In other words, the peak and the shoulder gradually approached each other and became more similar in shape as the concentration of the β crystalline form increased. In addition, some spectral changes also occurred in the fingerprint region. In Figure 4b, peaks at 1304, 1080, and 969 cm^{-1} developed along with the increase of β-form while peaks at 1277, 1047, and 950 cm^{-1} receded into shoulders. Similar observations have been made in other studies.[8] These observations are important because they demonstrate a correlation between the presence of the metastable β-structure (confirmed by WAXD) and the changes, especially the appearance of new bands, in the vibrational spectra. As a result, those peaks mentioned above could be regarded as indicators of the presence of the planar zigzag backbone characteristic of the β crystalline polymorph.

Studies on Single Fibers. Selected area electron diffraction (SAED) via low dose TEM was used to examine the crystal structure and orientation at the single fiber scale. Figure 5 shows the bright-field images and SAED patterns of individual electrospun PHBHx fibers collected on aluminum foil (a, a′), across the air gap (b, b′), and on the tapered edge of the rotary disk (c, c′). The fibers from the air gap (b) and the rotary disk (c) were comparable in size with diameters of 195 and 221 nm, respectively, while the fiber from the aluminum foil (a) was 2 times bigger with a diameter of 495 nm. The corresponding SAED patterns of these three fibers showed clear differences from each other, although all three SAED patterns had crystalline reflections characteristic of the orthorhombic α-form crystals, the orientation of the crystals changed significantly when using different collectors. In this study, the crystalline orientation is quantified by the tangential spread of electron diffraction or the degree of the central angles (ψ) of the equatorial $\alpha(020)$ and $\alpha(110)$, meridional $\alpha(002)$, and layer $\alpha(111)$ arc-shaped reflections, which are summarized in Table 2. The central angle of the arcs corresponds to the angular distribution of the indexed crystallographic planes,[47,48] so smaller ψ indicates higher degree of uniaxial orientation of the crystals. From Table 2, it is noted that the fiber from the rotary disk always exhibited the smallest ψ for all arcs, suggesting that in this single fiber the α-form crystals had the highest degree of orientation among the three samples, and the polymeric chains in the crystals were highly oriented along the fiber axis. The crystalline reflection of the β-form crystals appeared in fibers from the two modified collectors where a pair of new equatorial arcs were observed in both 4b′ and 4c′, which are assigned to the β-form crystal plane. Since the β-form crystal structure is a strain-induced paracrystalline structure, this observation indicates that the two modified collectors indeed introduced extra stretching forces on the fibers which are strong enough to stretch the polymer chains to an essentially fully extended form. It is also noted that the β-form arcs always had a small central angle of 8° (Table 2), suggesting a high orientation of the molecular chains in the β-crystals along the fiber axis under different collection conditions.

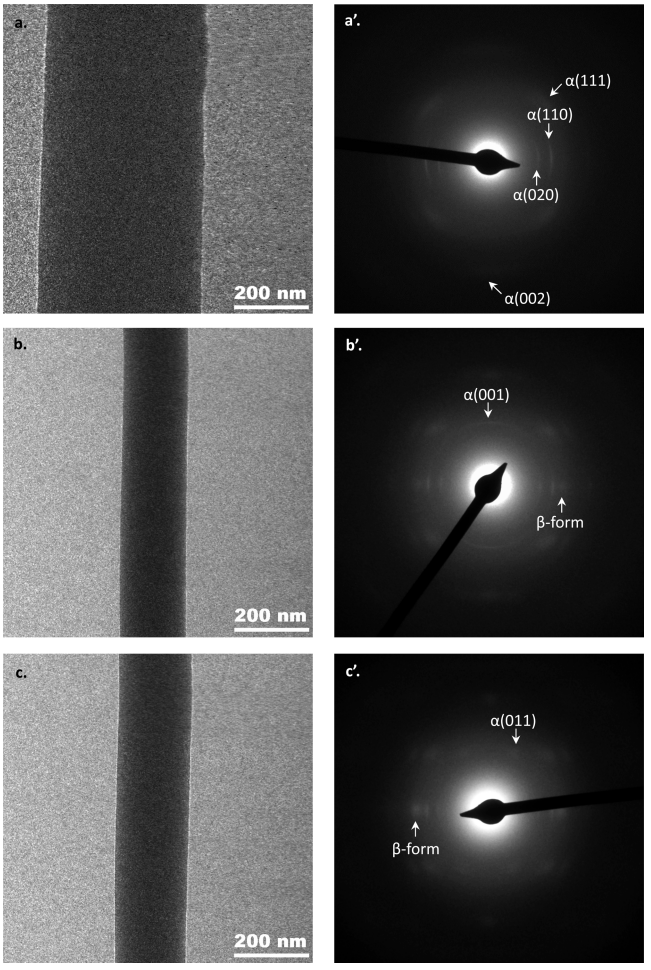

Figure 5. Bright-field TEM images of single electrospun PHBHx nanofibers from different collectors (a–c) and their corresponding SAED patterns (a′–c′).

For each of the three SAED patterns, the intensity profile along the equatorial line was plotted against the scattering vector ($1/d$, reciprocal of space distance), and the profiles obtained are shown in Table 2. In order to eliminate the influence of nonstructure-related factors, such as electron beam conditions and photorecording conditions, the background gray values for all three SAED patterns were equalized before analysis. The baseline was corrected by fitting the background for each of the profiles. The following observations were made from these intensity profiles, first, from left to right, the intensities of the $\alpha(020)$ and $\alpha(110)$ peaks both decreased while the intensity of the β peak increased, indicating a decrease in the α-crystal structure content and a correlated increase in the β-crystal structure content. These observations indicate that the stretching forces from the insulated gap, which are caused by the electrostatic attraction between the positively charged fibers and the negatively charged gap edges and the electrostatic repulsion between the residual positive charges on each fiber, are significantly weaker than those from the rotary disk. In addition, the correlated increase of the β-crystal content along with the decrease of the α-crystal content suggests that the formation of the β-form crystal structure is initiated by the stretching forces from the two modified collectors, and the α- and β-form crystal structures were formed simultaneously from amorphous and mobile polymer chains by two competing crystallization processes during collection. It is noted that this formation mechanism of the β-form crystal structure is different

DOI: 10.1021/acs.macromol.5b00638
Macromolecules XXXX, XXX, XXX–XXX

Table 2. Schematic of the SAED Patterns of Single Fibers Collected with Different Methods and Central Angles of the Arc Reflections of the Indexed Crystalline Planes

		Collector		
		Al foil	Air gap	Rotary disk
Schematic reflection pattern [a]		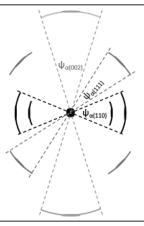	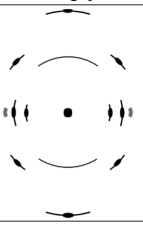	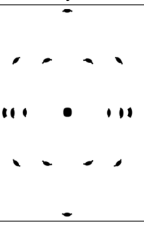
Central angle (ψ°)	α(020)	31	23	11
	α(110)	37	25	12
	α(111)	22	16	12
	α(002)	30	24	8
	β-form	-	8	8
SAED intensity profiles		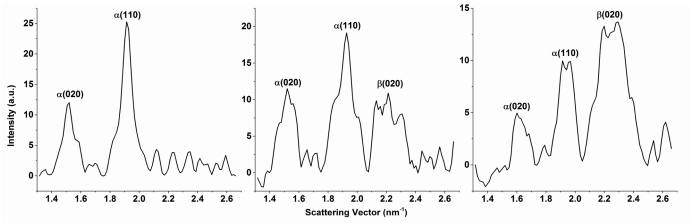		

[a]The intensities of the reflections are represented by the gray scale.

from those proposed by Iwata[12] and Ishii[22] in which the β-crystals are formed after the α-crystals. Second, the full width at half-maximum (fwhm) of the two α-peaks increased, indicating a decrease in the effective crystal size according to the Scherrer equation.[49] However, the fwhm of the β-peak in the last two profiles were similar, suggesting that the effective size of β-crystals remains the same when experiencing different stretching forces. The decrease of the effective sizes of the α-crystals may be due to faster solvent evaporation and thus more rapid solidification when using the modified collectors. As a result, the polymer chains were locked up at the initial state of crystallization. In short, the extra stretching forces provided by the modified collectors during the collection process would initiate the formation of the β-crystalline structure by extending the mobile amorphous chains to a planar zigzag conformation, which competes with the formation of the α-crystalline structure. In addition, these stretching forces would enhance the orientation of the α-crystals along the fiber axis and decrease their effective sizes. However, the influence of the stretching forces on the orientation degree and sizes of the β-crystals is limited.

When the SAED patterns in 5b′ and 5c′ were carefully examined, we found that for each indexed α-crystal plane listed in Table 2 there was always a superposition of two arcs with different widths in the azimuthal direction, especially in 5b′ (see schematics in Table 2). One arc had a larger central angle but was narrower, and the other one had a smaller central angle but was broader, indicating that there were two sets of α-crystals differing in orientation degree and crystal size. It was also observed that the narrower arc became much smaller as the stretching forces increased from 5a′ to 5c′ while the broader arc was only slightly smaller, indicating that the stretching had different influences on the orientation of the two sets of α-crystals. Another interesting observation was the appearance of a large α(001) layer line across the meridian in 5b′ while two pairs of distinct α(011) arc reflections were observed in 5c′. These results indicate a change in the packing states of the molecular chains in the α-form crystal structure along the fiber axis.

To summarize, the results from the SAED experiments on single fibers confirm a significant influence of the collection methods on the crystal structure and orientation level of the crystals, which is consistent with the conclusions drawn from the investigations on fiber bundles. Furthermore, the SAED results also demonstrated that substantial polymer chain orientation does occur even in randomly collected fibers on aluminum foil, something that could not be previously determined in fiber bundle studies.[50] These results further indicate that stretching forces during the electrospinning process are large enough to partially orient the chains but are not large enough to extend the chains to a planar zigzag conformation, which requires extra stretching forces during collection. In addition, in the SAED experiments, the rotary disk aligned fibers were observed to have the highest level of chain orientation. This is in contrast to the results obtained from polarized FT-IR experiments where the bundle of air gap aligned fibers apparently shows the highest level of chain orientation among all three samples. This discrepancy may be due to the misalignment and size/morphology nonuniformity (beads) of the rotary disk aligned fibers in the bundle which would cause averaging of the polarized FT-IR signals over fiber bundles. As a result, investigation of individual polymer nanofibers becomes increasingly more important.

As stated above, SAED is a powerful technique for the investigation of single electrospun nanofibers. However, SAED experiments are sometimes difficult and time-consuming.[50] To complement these results, we have used a novel technique, AFM-IR, which allows direct investigation of both the crystalline and amorphous phases of ultrafine electrospun fibers at the single fiber scale. AFM-IR is a technique combining

DOI: 10.1021/acs.macromol.5b00638
Macromolecules XXXX, XXX, XXX−XXX

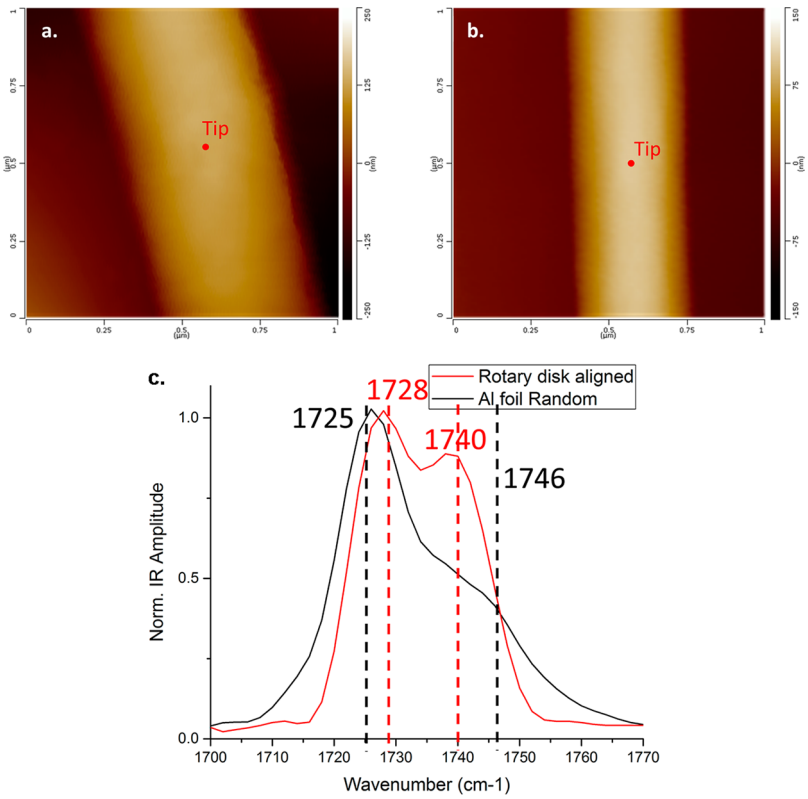

Figure 6. AFM images of single electrospun PHBHx fibers collected on (a) aluminum foil (473 nm) and (b) the tapered edge of a rotary disk (324 nm). (c) IR spectra of fibers shown in (a) and (b). The red dots on the two individual fibers indicate the position of the AFM tip.

atomic force microscopy (AFM) and infrared spectroscopy (IR) for nanoscale characterization. It provides IR spectra and AFM images simultaneously of sub-100 nm features. The source is a tunable IR laser whose wavelength can be swept through the infrared "fingerprint" region in less than 1 min. If one of the wavelengths is absorbed by the sample, then thermal expansion of the sample occurs on the nanosecond time scale, which causes a modulation of the oscillating AFM cantilever. This creates a "ringdown" at that particular frequency which decays as the heat dissipates. The positive amplitude of the oscillation represents the IR band intensity, and hence as the frequency is tuned through the IR region (900−3600 cm^{-1}), an IR spectrum is obtained at a spatial resolution of 50−100 nm. More details of this instrumentation are reported elsewhere.[51]

In order to test the feasibility of this technique, the IR spectra of a single Al foil fiber and a single rotary disk fiber were collected and compared with the transmission FT-IR spectra of their corresponding fiber mats (Figure 3, spectra in black and blue). Figures 6a and 6b are the AFM images of the two fibers with diameters of 473 and 324 nm, respectively. The IR spectra of these two single fibers are displayed in Figure 6c. As shown in the figure, the spectrum of the fiber collected on Al foil could be resolved into two features, an intense peak at 1725 cm^{-1} and a weak shoulder at 1746 cm^{-1}, corresponding to the α crystalline phase and the amorphous phase, respectively. However, in the spectrum of the fiber collected on a rotary disk, two distinct peaks at 1728 and 1740 cm^{-1} were observed, which were assigned respectively to the more ordered α crystalline phase and the β crystalline phase. These nano-IR spectra are in good agreement with the traditional FT-IR spectra in terms of peak/shoulder position and relative intensity. However, it is noted that the peaks in the nano-IR spectra are more highly resolved compared to the corresponding FT-IR spectra which are broadened and smeared due to averaging over a distribution of slightly misaligned fibers.

Generation Mechanism of the β-Form Crystal Structure. The generation of the β-form crystal structure could have a significant influence on various properties of the material. So far, this strain-induced metastable crystalline structure has been reported in highly crystallized materials of PHB and PHBV processed in different ways, including hot/cold drawn films, two-step-drawn fibers, and one-step-drawn fibers after isothermal crystallization.[22] In these highly stretched PHB or PHBV thin films and fibers, the β-form was believed to originate from the free chains in the amorphous phase between well-developed α lamellar crystals. In other words, the β-form crystal structure is generated after the formation of the α-crystals. However, by using similar processing methods, one cannot obtain the β-form crystal structure in PHBHx[52] because of the large amount of amorphous chains in the material that could not be highly extended during processing.

In our present work, we successfully generated the β-form crystalline structure in PHBHx by collecting the nanofibers on a high-speed-rotating disk, although the crystallinity of the resultant fibers is as low as 44 ± 1% as suggested by a preliminary DSC measurement (if the crystallinity is calculated with the equation $X_c = \Delta H_m/\Delta H_{m0} \times 100\%$, where ΔH_{m0} is the melting enthalpy of 100% crystalline PHB homopolymer (146 J/g[53])). On the basis of the experimental observations that the α- and β-form crystals coexist simultaneously in the resultant fibers and that the increase of the β-crystal content is correlated with the decrease of the α-crystal content with increasing stretching forces during collection (see SAED), we conclude that both the α and β crystalline forms are formed during

DOI: 10.1021/acs.macromol.5b00638
Macromolecules XXXX, XXX, XXX−XXX

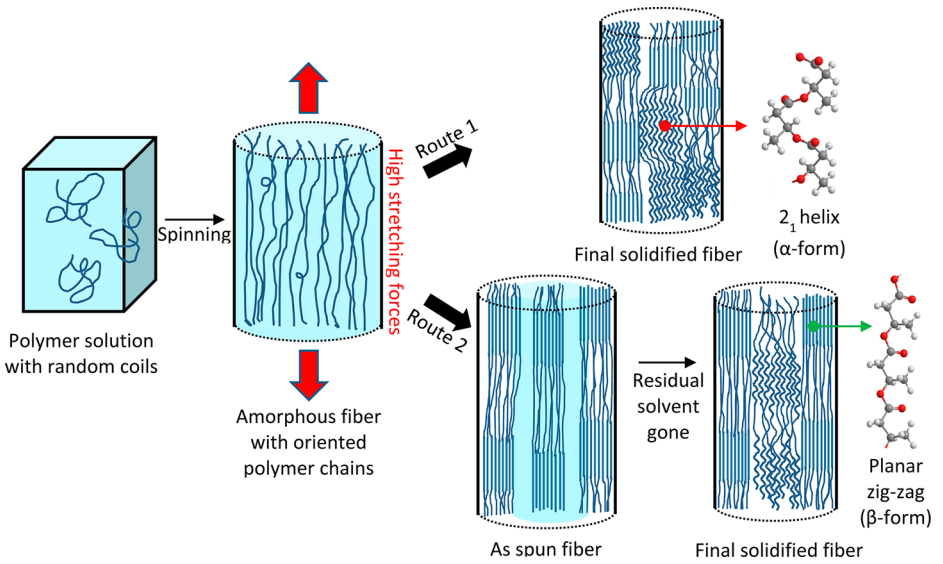

Figure 7. Two possible generation mechanisms for the formation of the α- and β-form crystal structure during electrospinning and collection. Route 1 indicates the simultaneous formation of the α- and β-crystalline forms during nanofiber collection. Route 2 indicates that the α-crystalline form is generated after the formation of the β-form. The α-crystalline form is originated from the relaxed planar zigzag chains (β-form) due to the existence of residual solvent in the core. In this figure, wavy lines in the fiber illustrate the 2_1 helical backbones of the chains in the α-phase, straight lines illustrate the planar zigzag backbones of the chains in the β-phase, and random curvy lines illustrate the free chains in the amorphous phase. Cyan color in the figure represents solvent.

collection. Both appear to be formed from amorphous and mobile chains by two distinct, competing crystallization processes. The possible generation mechanisms of the β-crystalline structure are illustrated in Figure 7. Unlike the generation mechanism reported previously (β-crystals are formed after the α-crystals), the β-form in the electrospun PHBHx nanofibers is actually formed at the same time as (route 1) or even before the formation of the α-form (route 2). The dissolved polymer chains in their random coil state are highly stretched during electrospinning and thus extended and oriented along the stretching direction. As a result, the amorphous fibers arriving at the air gap or rotary disk consist of oriented polymer chains along the fiber axis and are plasticized by remaining solvent. During collection, the amorphous fibers are further stretched by the additional elongational forces provided by stretching across a gap or by winding up on a high-speed rotating wheel. At the highest elongation, some oriented chains in the amorphous fiber would be fully extended and adopt a planar zigzag conformation. At high solvent evaporation rates, this metastable β-conformation would be locked in the solidified fiber, and thus β-crystals would be formed simultaneously with the α-crystals, as illustrated in route 1. An additional possibility is that under strong tensile forces during collection most of the polymer chains in the amorphous fiber are fully extended and adopt a planar zigzag conformation. At slower evaporation rates due to the trapping of residual solvent in the core of the as-spun fiber, a portion of the chains, especially in the core, would relax and convert to the more stable helical conformation (α-form). Therefore, the final solidified fibers would contain both the α- and β-crystalline structure, as illustrated in route 2. Realistically, the actual generation mechanism might be a combination of both, and ongoing studies will hopefully provide more insight into the formation process of the β-form in PHBHx.

CONCLUSION

A microstructural investigation of electrospun PHBHx nanofibers was conducted on fiber mats and on single nanofibers. The molecular chain conformation, the crystal structure, and the orientation of the crystals/chains were investigated by polarized-FT-IR, WAXD, SAED, and AFM-IR and were found to be highly dependent on the collection methods. More importantly, for the first time, the strain-induced β-form crystal structure was obtained in electrospun PHBHx nanofibers by using two modified collectors. The β-form was identified based on the appearance of a new crystalline reflection in WAXD and SAED and the spectral changes observed in the IR spectra. In addition, the results from the SAED experiments on individual fibers provided insights about the correlations between stretching forces and the degree of orientation and size of the α- and β-crystals. Finally, the AFM-IR technique was demonstrated to be a powerful and efficient tool for the microstructural investigation of individual electrospun nanofibers. In addition, according to the experimental results, we proposed a new generation mechanism of the β-form crystal structure which is significantly different from those previously reported. The β-crystals, originating from the oriented free chains in the fiber, were formed at the same time as or even before the formation of the α-crystals during collection. Our present study has led to an additional investigation of the relationship between the β-structure and the mechanical properties and processing protocols of PHBHx. The corresponding changes in the macroscopic performance of the material, together with its excellent biodegradability and biocompatibility, make PHBHx a promising material in many application areas.

AUTHOR INFORMATION

Corresponding Author

*E-mail rabolt@udel.edu; Ph +1-302-831-4476; Fax +1-302-831-4545 (J.F.R.).

DOI: 10.1021/acs.macromol.5b00638
Macromolecules XXXX, XXX, XXX−XXX

Notes

The authors declare no competing financial interest.

■ ACKNOWLEDGMENTS

The authors acknowledge support from Delaware NSF EPSCoR Grant # 1301765 and the NSF DMR Polymers Program Grant #1407255. D.C.M. thanks the NSF through Polymers Program Grant DMR-1103027. The authors also acknowledge C. J. McBrin for valuable insights and contributions to this work.

■ REFERENCES

(1) Chen, G.-Q. In *Plastics from Bacteria SE - 2*; Chen, G.-Q., Ed.; Microbiology Monographs; Springer: Berlin, 2010; Vol. *14*, pp 17−37.
(2) Noda, I.; Lindsey, S. B. B.; Caraway, D. In *Plastics from Bacteria SE - 10*; Chen, G. G.-Q., Ed.; Microbiology Monographs; Springer: Berlin, 2010; Vol. *14*, pp 237−255.
(3) Yoshie, N.; Saito, M.; Inoue, Y. *Macromolecules* **2001**, *34*, 8953−8960.
(4) Poliakoff, M.; Noda, I. *Green Chem.* **2004**, *6*, G37−G38.
(5) Yokouchi, M.; Chatani, Y.; Tadokoro, H.; Teranishi, K.; Tani, H. *Polymer* **1973**, *14*, 267−272.
(6) Laycock, B.; Halley, P.; Pratt, S.; Werker, A.; Lant, P. *Prog. Polym. Sci.* **2013**, *38*, 536−583.
(7) Iwata, T.; Tanaka, T. In *Plastics from Bacteria SE - 11*; Chen, G. G.-Q., Ed.; Microbiology Monographs; Springer: Berlin, 2010; Vol. *14*, pp 257−282.
(8) Murakami, R.; Sato, H.; Dybal, J.; Iwata, T.; Ozaki, Y. *Polymer* **2007**, *48*, 2672−2680.
(9) Orts, W. J.; Marchessault, R. H.; Bluhm, T. L.; Hamer, G. K. *Macromolecules* **1990**, *23*, 5368−5370.
(10) Aoyagi, Y.; Doi, Y.; Iwata, T. *Polym. Degrad. Stab.* **2003**, *79*, 209−216.
(11) Iwata, T.; Tsunoda, K.; Aoyagi, Y.; Kusaka, S.; Yonezawa, N.; Doi, Y. *Polym. Degrad. Stab.* **2003**, *79*, 217−224.
(12) Iwata, T.; Fujita, M.; Aoyagi, Y.; Doi, Y.; Fujisawa, T. *Biomacromolecules* **2005**, *6*, 1803−1809.
(13) Iwata, T.; Aoyagi, Y.; Fujita, M.; Yamane, H.; Doi, Y.; Suzuki, Y.; Takeuchi, A.; Uesugi, K. *Macromol. Rapid Commun.* **2004**, *25*, 1100−1104.
(14) Furuhashi, Y.; Imamura, Y.; Jikihara, Y.; Yamane, H. *Polymer* **2004**, *45*, 5703−5712.
(15) Antipov, E. M.; Dubinsky, V. A.; Rebrov, a. V.; Nekrasov, Y. P.; Gordeev, S. A.; Ungar, G. *Polymer* **2006**, *47*, 5678−5690.
(16) Iwata, T.; Aoyagi, Y.; Tanaka, T.; Fujita, M.; Takeuchi, A.; Suzuki, Y.; Uesugi, K. *Macromolecules* **2006**, *39*, 5789−5795.
(17) Tanaka, T.; Fujita, M.; Takeuchi, A.; Suzuki, Y.; Uesugi, K.; Ito, K.; Fujisawa, T.; Doi, Y.; Iwata, T. *Macromolecules* **2006**, *39*, 2940−2946.
(18) Tanaka, T.; Yabe, T.; Teramachi, S.; Iwata, T. *Polym. Degrad. Stab.* **2007**, *92*, 1016−1024.
(19) Kabe, T.; Tsuge, T.; Kasuya, K.; Takemura, A.; Hikima, T.; Takata, M.; Iwata, T. *Macromolecules* **2012**, *45*, 1858−1865.
(20) Kabe, T.; Tsuge, T.; Hikima, T.; Takata, M.; Takemura, A.; Iwata, T. Processing, Mechanical Properties, and Structure Analysis of Melt-Spun Fibers of P(3HB)/UHMW-P(3HB) Identical Blend. In *Biobased Monomers, Polymers, and Materials*; ACS Symposium Series 1105; American Chemical Society: Washington, DC, 2012, 63−75.
(21) Tanaka, F.; Doi, Y.; Iwata, T. *Polym. Degrad. Stab.* **2004**, *85*, 893−901.
(22) Ishii, D.; Lee, W.-K.; Kasuya, K.-I.; Iwata, T. *J. Biotechnol.* **2007**, *132*, 318−324.
(23) Fukada, E.; Ando, Y. *Int. J. Biol. Macromol.* **1986**, *8*, 361−366.
(24) Huang, Z.-M.; Zhang, Y.-Z.; Kotaki, M.; Ramakrishna, S. *Compos. Sci. Technol.* **2003**, *63*, 2223−2253.
(25) Doshi, J.; Reneker, D. H.; Process, E. *J. Electrost.* **1995**, *35*, 151−160.
(26) Reneker, D. H.; Chun, I. *Nanotechnology* **1996**, *7*, 216−223.
(27) Li, D.; Xia, Y. *Adv. Mater.* **2004**, *16*, 1151−1170.
(28) Greiner, A.; Wendorff, J. H. *Angew. Chem., Int. Ed.* **2007**, *46*, 5670−5703.
(29) Huang, C.; Chen, S.; Lai, C.; Reneker, D. H.; Qiu, H.; Ye, Y.; Hou, H. *Nanotechnology* **2006**, *17*, 1558−1563.
(30) Reneker, D. H. H.; Yarin, A. L. L.; Zussman, E.; Xu, H. *Adv. Appl. Mech.* **2007**, *41*, 43−346.
(31) Chan, K. H. K.; Wong, S. Y.; Li, X.; Zhang, Y. Z.; Lim, P. C.; Lim, C. T.; Kotaki, M.; He, C. B. *J. Phys. Chem. B* **2009**, *113*, 13179−13185.
(32) Kongkhlang, T.; Tashiro, K.; Kotaki, M.; Chirachanchai, S. *J. Am. Chem. Soc.* **2008**, *130*, 15460−15466.
(33) Yee, W. A.; Kotaki, M.; Liu, Y.; Lu, X. *Polymer* **2007**, *48*, 512−521.
(34) Dror, Y.; Salalha, W.; Khalfin, R. L.; Cohen, Y. *Langmuir* **2003**, *19*, 7012−7020.
(35) Fennessey, S. F.; Farris, R. J. *Polymer* **2004**, *45*, 4217−4225.
(36) Ji, Y.; Li, C.; Wang, G.; Koo, J.; Ge, S.; Li, B.; Jiang, J.; Herzberg, B.; Klein, T.; Chen, S.; Sokolov, J. C.; Rafailovich, M. H. *EPL (Europhysics Lett.* **2008**, *84*, 56002.
(37) Kongkhlang, T.; Kotaki, M.; Kousaka, Y.; Umemura, T.; Nakaya, D.; Chirachanchai, S. *Macromolecules* **2008**, *41*, 4746−4752.
(38) Kimura, N.; Kim, H.-K.; Kim, B.-S.; Lee, K.-H.; Kim, I.-S. *Macromol. Mater. Eng.* **2010**, *295*, 1090−1096.
(39) Li, D.; Wang, Y.; Xia, Y.; Uni, V. *Nano Lett.* **2003**, *3*, 1167−1171.
(40) Kakade, M. V.; Givens, S.; Gardner, K.; Lee, K. H.; Chase, D. B.; Rabolt, J. F. *J. Am. Chem. Soc.* **2007**, *129*, 2777−2782.
(41) Jalili, R.; Morshed, M.; Ravandi, S. A. H. *J. Appl. Polym. Sci.* **2006**, *101*, 4350−4357.
(42) Ma, X.; Liu, J.; Ni, C.; Martin, D. C.; Chase, D. B.; Rabolt, J. F. *ACS Macro Lett.* **2012**, *1*, 428−431.
(43) Stephens, J. S.; Chase, D. B.; Rabolt, J. F. *Macromolecules* **2004**, *37*, 877−881.
(44) Chaurey, V.; Chiang, P.-C.; Polanco, C.; Su, Y.-H.; Chou, C.-F.; Swami, N. S. *Langmuir* **2010**, *26*, 19022−19026.
(45) Cai, H.; Qiu, Z. *Phys. Chem. Chem. Phys.* **2009**, *11*, 9569−9577.
(46) Cheng, M.-L.; Lin, C.-C.; Su, H.-L.; Chen, P.-Y.; Sun, Y.-M. *Polymer* **2008**, *49*, 546−553.
(47) Yoshioka, T.; Dersch, R.; Greiner, A.; Tsuji, M.; Schaper, A. K. *Macromol. Mater. Eng.* **2010**, *295*, 1082−1089.
(48) Yoshioka, T.; Dersch, R.; Tsuji, M.; Schaper, A. K. *Polymer* **2010**, *51*, 2383−2389.
(49) Lin, D. Y.-S. *Orientation and morphology development in electrospun nanofibers*, Ph.D. Dissertation, University of Michigan, 2005.
(50) Richard-Lacroix, M.; Pellerin, C. *Macromolecules* **2013**, *46*, 9473−9493.
(51) Dazzi, A.; Prater, C. C. B.; Hu, Q.; Chase, D. B.; Rabolt, J. F.; Marcott, C. *Appl. Spectrosc.* **2012**, *66*, 1365−1384.
(52) Josefine Fischer, J.; Aoyagi, Y.; Enoki, M.; Doi, Y.; Iwata, T. *Polym. Degrad. Stab.* **2004**, *83*, 453−460.
(53) Barham, P. J.; Keller, A.; Otun, E. L.; Holmes, P. A. *J. Mater. Sci.* **1984**, *19*, 2781−2794.

DOI: 10.1021/acs.macromol.5b00638
Macromolecules XXXX, XXX, XXX−XXX